Experimental study of the $\gamma p \to \pi^0 \pi^0 p$ reaction with the Crystal Ball/TAPS detector system at the Mainz Microtron

V. L. Kashevarov,[1,2,*] A. Fix,[3,†] S. Prakhov,[4] P. Aguar-Bartolomé,[1] J. R. M. Annand,[5] H. J. Arends,[1] K. Bantawa,[6] R. Beck,[7] V. Bekrenev,[8] H. Berghäuser,[9] A. Braghieri,[10] W. J. Briscoe,[11] J. Brudvik,[4] S. Cherepnya,[2] R. F. B. Codling,[5] E. J. Downie,[1,5] P. Drexler,[9] L. V. Fil'kov,[2] D. I. Glazier,[12] R. Gregor,[9] E. Heid,[1,11] D. Hornidge,[13] L. Isaksson,[14] I. Jaegle,[15] O. Jahn,[1] T. C. Jude,[12] I. Keshelashvili,[15] R. Kondratiev,[16] M. Korolija,[17] M. Kotulla,[9] A. Koulbardis,[8] S. Kruglov,[8] B. Krusche,[15] V. Lisin,[16] K. Livingston,[5] I. J. D. MacGregor,[5] Y. Maghrbi,[15] D. M. Manley,[6] J. C. McGeorge,[5] E. F. McNicoll,[5] D. Mekterovic,[17] V. Metag,[9] A. Mushkarenkov,[10] B. M. K. Nefkens,[4] A. Nikolaev,[7] R. Novotny,[9] H. Ortega,[1] M. Ostrick,[1] P. Ott,[1] P. B. Otte,[1] B. Oussena,[1] P. Pedroni,[10] F. Pheron,[15] A. Polonski,[16] J. Robinson,[5] G. Rosner,[5] T. Rostomyan,[10,‡] S. Schumann,[1,7] M. H. Sikora,[12] D. I. Sober,[18] A. Starostin,[4] I. I. Strakovsky,[11] I. M. Suarez,[4] I. Supek,[17] C. M. Tarbert,[12] M. Thiel,[9] A. Thomas,[1] M. Unverzagt,[1,7] D. P. Watts,[12] D. Werthmüller,[15] and F. Zehr[15]

(Crystal Ball at MAMI, TAPS, and A2 Collaborations)

[1]*Institut für Kernphysik, Johannes Gutenberg-Universität Mainz, D-55099 Mainz, Germany*
[2]*Lebedev Physical Institute, 119991 Moscow, Russia*
[3]*Laboratory of Mathematical Physics, Tomsk Polytechnic University, Tomsk, Russia*
[4]*University of California Los Angeles, Los Angeles, California 90095-1547, USA*
[5]*Department of Physics and Astronomy, University of Glasgow, Glasgow G12 8QQ, United Kingdom*
[6]*Kent State University, Kent, Ohio 44242-0001, USA*
[7]*Helmholtz-Institut für Strahlen- und Kernphysik, University of Bonn, D-53115 Bonn, Germany*
[8]*Petersburg Nuclear Physics Institute, 188350 Gatchina, Russia*
[9]*II Physikalisches Institut, University of Giessen, D-35392 Giessen, Germany*
[10]*INFN Sesione di Pavia, I-27100 Pavia, Italy*
[11]*The George Washington University, Washington, DC 20052-0001, USA*
[12]*School of Physics, University of Edinburgh, Edinburgh EH9 3JZ, United Kingdom*
[13]*Mount Allison University, Sackville, New Brunswick E4L 1E6, Canada*
[14]*Lund University, SE-22100 Lund, Sweden*
[15]*Institut für Physik, University of Basel, CH-4056 Basel, Switzerland*
[16]*Institute for Nuclear Research, 125047 Moscow, Russia*
[17]*Rudjer Boskovic Institute, HR-10000 Zagreb, Croatia*
[18]*The Catholic University of America, Washington, DC 20064, USA*

The $\gamma p \to \pi^0 \pi^0 p$ reaction has been measured from threshold to 1.4 GeV using the Crystal Ball and TAPS photon spectrometers together with the photon tagging facility at the Mainz Microtron. The experimental results include total and differential cross sections as well as specific angular distributions, which were used to extract partial-wave amplitudes. In particular, the energy region below the $D_{13}(1520)$ resonance was studied.

I. INTRODUCTION

Although studied for a long time, the properties of many baryon resonances are still not well known, and a clear understanding of resonances in QCD is still not possible. Some states below 2.5 GeV are believed to couple strongly to final states with two pseudoscalar mesons. Therefore, the investigation of $\pi\pi$ and $\pi\eta$ photoproduction provides important new information about the nucleon excitation spectrum.

During the last two decades, an extensive study of double-pion photoproduction for $E_\gamma < 1$ GeV has been undertaken [1–14]. The theoretical interpretation of the data in various isospin channels was carried out using different phenomenological analyses [15–20]. As a rule, the models for double-pion production are based on isobar models or effective field theories. Typically, the reaction amplitude is constructed as a sum of background and resonance contributions. The background part contains nucleon Born terms as well as meson exchange in the t channel. The resonance part is a coherent sum of s-channel resonances decaying into $\pi\pi N$ via intermediate formation of meson-nucleon and meson-meson states ("isobars"). Despite significant qualitative differences between the models, in general they provide an acceptable description of the existing cross-section data. Such an apparent consistency between theoretical models does not indicate a high level in understanding double-pion photoproduction; rather it demonstrates a weak sensitivity of the existing data to the underlying dynamics.

The reaction $\gamma p \to \pi^0 \pi^0 p$ is a typical example where the data on double-pion production have not been fully

*kashev@kph.uni-mainz.de
†fix@mph.phtd.tpu.ru
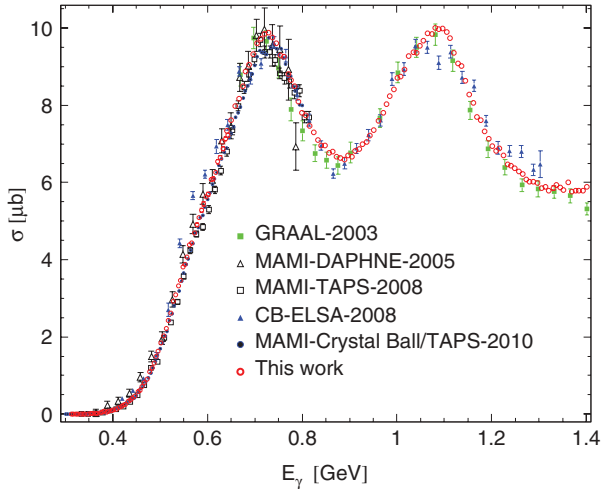‡Present address: Institut für Physik, University of Basel, Switzerland.

FIG. 1. (Color online) Total cross sections for $\gamma p \to \pi^0 \pi^0 p$ are shown as a function of the incident-photon energy. The results obtained in this work are compared to the existing data from GRAAL [6], CB-ELSA [11,12], DAPHNE [8], TAPS [12], and Crystal Ball/TAPS [40]. Only statistical uncertainties are shown for all data.

understood theoretically, especially below the second resonance region. A widely accepted property of this reaction is a large contribution from $D_{13}(1520)$, which is known to couple strongly to the $\pi \Delta$ channel [21,22]. The $D_{13}(1520)$ contribution to the $\gamma p \to \pi^0 \pi^0 p$ total cross section is seen as the first peak at $E_\gamma \approx 730$ MeV (see Fig. 1), the features of which are reproduced more or less successfully by all models. However, the dynamics underlying this reaction in the region from the $D_{13}(1520)$ resonance down to threshold have not been well understood so far. In this region, the total cross section demonstrates an almost linear rise, hinting at s-wave dominance in the final state, which, however, is not confirmed by the theory. An attempt to describe such behavior by a large contribution of the Roper resonance $P_{11}(1440)$, decaying into σN in s wave [16], seems to be ruled out by subsequent investigations [12,15,17,19,20]. The $D_{13}(1520)$ contribution itself, according to the results of Refs. [12,17,19], reduces rapidly with decreasing energy and cannot explain the experimental data in the region below $E_\gamma = 650$ MeV. In Ref. [12], the authors try to describe the $\gamma p \to \pi^0 \pi^0 p$ reaction by a dominant contribution from the $D_{33}(1700)$ resonance. The well-known minimum at $W = 1.6$ GeV and the second maximum at $W = 1.7$ GeV, seen in the $\gamma p \to \pi^0 \pi^0 p$ total cross section, were described in Ref. [12] by the interference between $D_{13}(1520)$ and $D_{33}(1700)$. However, a simple consideration using the Clebsch-Gordan coefficients shows that $\pi \Delta$ photoproduction in the $I = 3/2$ channel should lead to the ratio

$$
\begin{aligned}
\frac{\sigma(\pi^+ \pi^- p)}{\sigma(\pi^0 \pi^0 p)} &\approx \frac{\sigma(\pi^- \Delta^{++}) + \sigma(\pi^+ \Delta^0)}{\sigma(\pi^0 \Delta^+)} \\
&= \left\{ \left(C_{1-1\frac{3}{2}\frac{3}{2}}^{\frac{3}{2}\frac{1}{2}} C_{11\frac{3}{2}\frac{1}{2}}^{\frac{3}{2}\frac{3}{2}} \right)^2 + \left(C_{11\frac{3}{2}-\frac{1}{2}}^{\frac{3}{2}\frac{1}{2}} C_{1-1\frac{1}{2}\frac{1}{2}}^{\frac{3}{2}-\frac{1}{2}} \right)^2 \right\} \\
&\quad : \left(C_{10\frac{3}{2}\frac{1}{2}}^{\frac{3}{2}\frac{1}{2}} C_{10\frac{1}{2}\frac{1}{2}}^{\frac{3}{2}\frac{1}{2}} \right)^2 = 13,
\end{aligned}
\tag{1}
$$

where for simplicity we neglect the interference between two possible πN pairs. Taking a value $\sigma = 4\ \mu$b for the $D_{33}(1700)$ contribution to $\pi^0 \pi^0 p$, as predicted in Ref. [12], assumes that at least 70% of the $\gamma p \to \pi^+ \pi^- p$ total cross section comes from this resonance alone, which seems unlikely. The major (about 80%) part of the $\gamma p \to \pi^+ \pi^- p$ total cross section comes from the Δ-Kroll-Ruderman term, so that the addition of such a strong contribution from $D_{33}(1700)$ would result in a significant overestimation of the experimental data. Thus the dynamics of double-π^0 photoproduction in the energy region below $D_{13}(1520)$ are still far from being well understood.

Major disagreements between the results of different models as well as between the theoretical predictions and the experimental data were revealed in Refs. [9,13], in which the measurement of the beam helicity asymmetry $I^\odot$ for $\pi^+ \pi^-$, $\pi^+ \pi^0$, and $\pi^0 \pi^0$ was reported. As discussed in Ref. [23], this quantity is very sensitive to the model details, so that even a small variation of the model parameters can change the results significantly. However, the interpretation of polarization measurements in terms of the spin and parity of J^P is quite difficult, especially for the processes with more than two particles in the final state. Therefore, it is desirable to find a method that, on the one hand, will be sensitive to the details of the dynamical structure and, on the other hand, will provide a clear interpretation of the results in terms of spin parity of the contributing waves. Furthermore, especially important is that the method should not be connected strictly to the isobar model, allowing one to perform the partial-wave analysis with a minimal model dependence. An approach that seems to obey the requirements discussed above was applied for analysis of inelastic pion-nucleon scattering $\pi N \to \pi \pi N$ (see, for example, Refs. [24,25]). A similar formalism for photoproduction of two pseudoscalars was developed in Ref. [26]. Such approaches require high-statistics data covering the full solid angle. In the present work, we remeasured double-π^0 photoproduction off the proton with an unprecedented accuracy and applied the formalism of Ref. [26] to study its dynamics, having a main goal to learn which J^P waves dominate in this reaction at the energies below $D_{13}(1520)$.

The experimental data in the present study were obtained at the Mainz tagger photon facility using an almost 4π detector based on the Crystal Ball and TAPS multiphoton spectrometers.

This paper includes a brief description of the experimental setup, data handling, the model formalism, discussion of the results, and conclusions.

II. EXPERIMENTAL SETUP

The reaction $\gamma p \to \pi^0 \pi^0 p$ was studied using the Crystal Ball (CB) [27] as the central spectrometer and TAPS [28,29] as a forward spectrometer. These detectors were installed in the energy-tagged bremsstrahlung photon beam of the Mainz Microtron (MAMI) [30,31]. The photon energies were determined by the Glasgow tagging spectrometer [32–34].

The CB detector is a sphere consisting of 672 optically insulated NaI(Tl) crystals, shaped as truncated triangular

pyramids, which point toward the center of the sphere. The crystals are arranged in two hemispheres that cover 93% of 4π sr, sitting outside a central spherical cavity with a radius of 25 cm, which is designed to hold the target and inner detectors. In this experiment, TAPS was arranged in a plane consisting of 384 BaF_2 counters of hexagonal cross section. It was installed 1.5 m downstream of the CB center covering the full azimuthal range for polar angles from $1°$ to $20°$. More details on the energy and angular resolution of the CB and TAPS are given in Refs. [35,36].

The present measurement used 855-MeV and 1508-MeV electron beams from the upgraded Mainz Microtron, MAMI-C [31]. The data with the 1508-MeV beam were taken in 2007, and with the 855-MeV beam in 2008. Bremsstrahlung photons, produced by the 1508-MeV electrons in a 10-μm Cu radiator and collimated by a 4-mm-diameter Pb collimator, were incident on a 5-cm-long liquid hydrogen (lH_2) target located in the center of the CB. The energies of the incident photons were measured in the range 617 to 1402 MeV by detecting the post-bremsstrahlung electrons in the Glasgow tagger [32]. With the 855-MeV electron beam, bremsstrahlung photons were produced in a diamond radiator, collimated by a 3-mm-diameter Pb collimator, and incident on a 10-cm-long lH_2 target. In this experiment, the energies of the incident photons were tagged from 84 to 796 MeV. The energy resolution of the tagged photons is mostly defined by the width of the tagger focal plane detectors, and by the electron beam energy. For a beam energy of 1508 MeV, a typical width of a tagger channel was about 4 MeV, and about 2 MeV for a beam energy of 855 MeV. Due to the beam collimation, only part of the bremsstrahlung photon flux reached the lH_2 target. In order to evaluate the reaction cross sections, the probability of bremsstrahlung photons reaching the target (the so-called tagging efficiency) was measured for each tagger channel. The typical tagging efficiency in the experiment with the 1508-MeV electron beam was found to vary between 67% and 71%. With the 855-MeV electron beam, the tagging efficiency varied with photon energy between 30% and 60%.

The experimental trigger in the measurement with the 1508-MeV electron beam required the total-energy deposit in the CB to exceed $\sim$320 MeV and the number of so-called hardware clusters in the CB to be larger than two. With the 855-MeV electron beam, the trigger required the total energy in the CB to exceed $\sim$100 MeV, and the number of hardware clusters in the CB and TAPS together to be larger than 1, with at least one hardware cluster in the CB.

More details on the experimental conditions of the data taking with the 1508-MeV electron beam in 2007 are given in Refs. [35,36].

III. DATA ANALYSIS

The reaction $\gamma p \rightarrow \pi^0\pi^0 p$ was identified using events with four photons detected in the calorimeters. There were two independent analyses made to cross-check the results. In the first analysis, the event-selection procedure was similar to the one that was used to measure the reaction $\gamma p \rightarrow \pi^0\eta p$ [37]. The second analysis was based on the kinematic-fit technique

and was similar to those published in Refs. [35,36]. Both analyses are in excellent agreement. Since the kinematic-fit technique typically yields data with better resolution, the results of the second analysis were used.

The details of the kinematic-fit parametrization of the detector information and resolution were given in Ref. [35]. The four- and five-cluster events that satisfied the hypothesis of the process $\gamma p \rightarrow \pi^0\pi^0 p \rightarrow 4\gamma p$ at the 2% confidence level, CL, (i.e., with a probability of misinterpretation less than 2%) were accepted as the reaction candidates. The kinematic-fit output for which the pairing combination of the four photons to two π^0s had the largest CL was used to reconstruct the reaction kinematics. Possible background from other reactions was checked by their simulation and by determination of a probability for them to be misidentified as $2\pi^0$ events. Below the $\gamma p \rightarrow \pi^0\eta p$ threshold, the background contamination was found to be only from interaction of incident photons in the windows of the target cell and from random coincidences. This contamination was subtracted from the experimental spectra by using data samples with random coincidences and with an empty (no liquid hydrogen) target. The background from the $\gamma p \rightarrow \pi^0\eta p \rightarrow 4\gamma p$ events was estimated to be quite small, reaching only 0.5% at incident-photon energies of 1.4 GeV. So this background was neglected in our results.

The determination of the experimental acceptance was based on a Monte Carlo (MC) simulation of the $\gamma p \rightarrow \pi^0\pi^0 p$ reaction with different event generators based on various assumptions about the reaction dynamics. For the most part, the MC simulation was made as the process $\gamma p \rightarrow \Delta\pi^0 \rightarrow \pi^0\pi^0 p$, using the mass (1210 MeV) and width (100 MeV) of the Delta resonance at its pole position (Ref. [38]). With these parameters, the agreement between the experimental and MC-simulation distributions of the invariant mass $m(\pi^0 p)$ is much better than that obtained when the Breit-Wigner parameters of Δ from Ref. [38] are used. The same parameters also give a good description of the Δ peak seen in the reaction $\pi^- p \rightarrow \pi^0\pi^0 n$ [39]. One simulation was made by generating an isotropic angular distribution of the $\Delta \rightarrow \pi^0 p$ decay. Another was made similar to the experimental angular distribution in the region of the first peak in the $\gamma p \rightarrow \pi^0\pi^0 p$ total cross section (see Fig. 1). Part of the MC simulation modelled the process $\gamma p \rightarrow D_{13}(1520)\pi^0 \rightarrow \pi^0\pi^0 p$, where the D_{13} mass and width were taken as 1510 MeV and 110 MeV, respectively. This simulation was used only in the analysis of the data taken with the 1508-MeV electron beam and only for the energies in which the $\gamma p \rightarrow D_{13}(1520)\pi^0 \rightarrow \pi^0\pi^0 p$ contribution becomes visible. For these energies, the determination of the experimental acceptance was done by mixing the Δ and D_{13} simulations, where the weights of each simulation were adjusted to get the best agreement with the experimental $m(\pi^0 p)$ distributions. The comparison of the measured and simulated $m^2(\pi^0 p)$ distributions is shown in Fig. 2 for four different energies. The agreement between the measured and simulated distributions is better at lower energies. This agreement is almost independent of the choice of the angular distribution used for the Δ-decay simulation; it affects only the shape of the $m(\pi^0\pi^0)$ spectrum. The resonance peaks seen in the $m^2(\pi^0 p)$ spectra look different from the Breght-Wigner shape, as every event is represented
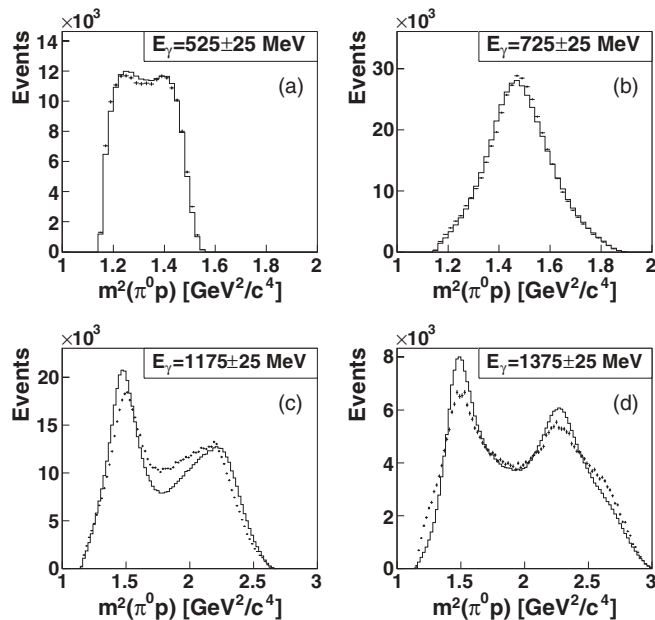
FIG. 2. Experimental $m^2(\pi^0 p)$ invariant-mass distributions (crosses) compared to those obtained from the MC simulation (solid line) of the $\gamma p \to \pi^0 \pi^0 p$ reaction. The MC event generation included the $\Delta \pi^0$ and $D_{13}(1520)\pi^0$ intermediate states in double-π^0 photoproduction.

by two $m^2(\pi^0 p)$ values, which are located symmetrically in the $\pi^0 \pi^0 p$ Dalitz plot with respect to its symmetry line (see Ref. [39] and its Fig. 6 for more details). Then every resonance band in the Dalits plot has its reflection with respect this symmetry line. In Fig. 2(a) for example, the projection of the Δ band to the $m^2(\pi^0 p)$ axis is seen in the right part of the spectrum, while a bump in the left part just corresponds to the reflection of the Δ band with respect to the symmetry line.

For the data at each electron-beam energy, the corresponding MC events were propagated through a GEANT (version 3.21) simulation of the experimental setup, folded with resolutions of the detectors and conditions of the trigger. The resulting simulated data were then analyzed in the same way as the experimental data. The average acceptance for the data with the 855-MeV electron beam was found to be close to 60% for the entire energy range of double-π^0 photoproduction. The average acceptance for the data with the 1508-MeV electron beam decreases smoothly from 55% at $E_\gamma = 617$ MeV to 42% at $E_\gamma = 1400$ MeV.

The total cross sections obtained from the $\gamma p \to \pi^0 \pi^0 p$ reaction are shown in Fig. 1 as a function of the incident-photon energy and are compared to some previous measurements. The majority of previous $\gamma p \to \pi^0 \pi^0 p$ experiments were at MAMI [1–3,7,8,12,40]. In Fig. 1, we include only the most recent results obtained with three different experimental setups: DAPHNE [8], TAPS [12], and Crystal Ball/TAPS [40]. The other measurements were performed at ELSA [11,12] and by GRAAL [6]. The results obtained in this work are in good agreement with all previous measurements within the given statistical and systematic uncertainties. It was possible with our new data to reduce considerably the energy binning
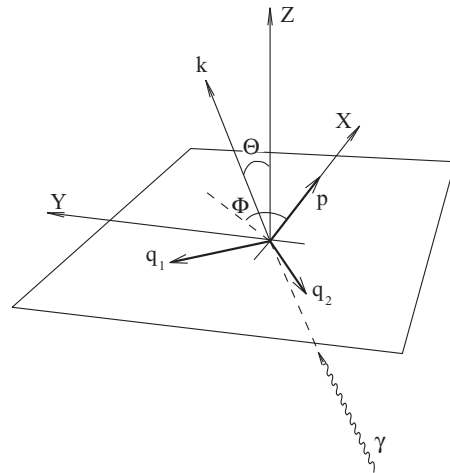

FIG. 3. Definition of the coordinate system used in the present formalism. $\vec{k}$, $\vec{p}$, $\vec{q}_1$, and $\vec{q}_2$ are respectively three-momenta of the incident-photon, out-going proton, two pions in the center of mass system. Axis Z is a normal to the decay plane. Axis X is along $\vec{p}$. Θ and Φ are respectively the polar and azimuthal angles of $\vec{k}$.

as well as the statistical uncertainties. The agreement of our total-cross-section results from the two measurements with different electron-beam energies can be seen in the overlapping range from $E_\gamma = 617$ MeV to $E_\gamma = 796$ MeV (shown later in Fig. 7).

The systematic uncertainties in the total and differential cross sections were estimated to be not larger than 6% and are dominated by the determination of the experimental acceptance for $\gamma p \to \pi^0 \pi^0 p$ and the photon-beam flux. The systematic uncertainty because of the acceptance determination was studied by comparing our results for the total cross sections that were obtained with various MC simulations based on event generators with different $\gamma p \to \pi^0 \pi^0 p$ dynamics. Also, we compared the total cross sections that were obtained from the integration of the differential cross sections, which will be shown later in the text. The systematic uncertainty in the photon-beam flux was determined mostly by the variation of the tagging efficiency during the data-taking period.

IV. THE MODEL

The formalism used to interpret our experimental data is described in Ref. [26], where the formal expressions are derived for the helicity amplitude as well as for the cross section. At a particular photon energy, the reaction amplitude is determined by four independent continuous variables for unpolarized experiments, described below, and two discrete variables, which are taken as the initial and final helicities of the nucleon. Our choice of coordinate system is shown in Fig. 3, where all particles are in the center-of-mass frame. Axis Z is chosen along the normal to the decay plane, which is defined by the three final-state particles. Axis X is chosen along the outgoing-nucleon momentum. Angles Φ and Θ defined in Fig. 3 specify the direction of the incident-photon momentum $\vec{k}$ in this coordinate system. Together with the two angles, the energies of the two pions, ω_1 and ω_2, uniquely determine the

final-state kinematics. The angular dependence of the matrix element is then given [26] by

$$T_{\nu\mu}(\omega_1, \omega_2; \Phi, \Theta) = \sum_{JM} t_{\nu\mu}^{JM}(\omega_1, \omega_2) D_{M\mu}^{J}(\Phi, \Theta, -\Phi), \quad (2)$$

where $D_{m_1 m_2}^{j}$ are the Wigner functions and JM denote respectively the total angular momentum and its projection on axis Z. The complex partial amplitudes $t_{\nu\mu}^{JM}$, which depend on the energies ω_1 and ω_2, contain the full dynamics of the process.

After spin summation and appropriate integration over ω_1 and ω_2, one obtains the unpolarized differential cross section $d\sigma/(d\cos\Theta\, d\Phi)$ or the corresponding normalized quantity [26]

$$W(\Theta, \Phi) \equiv \frac{1}{\sigma}\frac{d\sigma}{d\Omega}$$
$$= \sum_{L \geqslant 0}\sum_{M=-L}^{L}\sqrt{\frac{2J+1}{4\pi}}\,W_{LM}Y_{LM}(\Theta, \Phi), \quad (3)$$

which is expanded over spherical harmonics with $W_{00} = 1$. The coefficients W_{LM} in Eq. (3) are hermitian combinations of the partial-wave amplitudes $t_{\nu\mu}^{JM}$. The corresponding expression was obtained in Ref. [26]:

$$W_{LM} = \frac{\pi}{\sigma}\mathcal{K}\int d\omega_1 d\omega_2 \sum_{\nu\mu}\sum_{JJ'M_J M_J'}(-1)^{M+\mu}$$
$$\times C_{J'M_J' JM_J}^{LM} C_{J'\mu J-\mu}^{L0} t_{\nu\mu}^{J'M_J'}(\omega_1, \omega_2)^* t_{\nu\mu}^{JM_J}(\omega_1, \omega_2), \quad (4)$$

where $\mathcal{K}$ is an appropriate phase space factor. Formula (3) determines the general structure of an angular distribution in a manner analogous to the expansion of the cross section for single-meson photoproduction in terms of the Legendre polynomials.

To limit the number of model parameters, only the lowest partial waves were used. Their choice is motivated by previous isobar-model analyses which demonstrated that only waves with $J \leqslant 3/2$ were important below $E_\gamma = 0.8$ GeV [15,17, 19].

Expansion (3) written for the case of $J \leqslant 3/2$ is

$$W(\Theta, \Phi) = \frac{1}{4\pi}\left\{1 - \frac{3}{\sqrt{2}}W_{11}P_1^1(\cos\Theta)\cos\Phi\right.$$
$$+ 5\left(W_{20}P_2^0(\cos\Theta) + \frac{1}{\sqrt{6}}W_{22}P_2^2(\cos\Theta)\cos 2\Phi\right)$$
$$- \frac{7}{3}\left(\sqrt{3}W_{31}P_3^1(\cos\Theta)\cos\Phi\right.$$
$$\left.\left. - \frac{1}{2\sqrt{5}}W_{33}P_3^3(\cos\Theta)\cos 3\Phi\right)\right\}, \quad (5)$$

from which it is easy to see that the $\cos\Theta$ distribution has a general form

$$W(\cos\Theta) = A + B\cos^2\Theta, \quad (6)$$

with

$$A = \frac{1}{2}\left(1 - \frac{5}{2}W_{20}\right), \quad B = \frac{15}{4}W_{20}. \quad (7)$$

As shown in Ref. [26], the identity of the two pions together with parity conservation results in the following symmetry relations:

$$W(\Theta, \Phi) = W(\pi - \Theta, \Phi) = W(\Theta, 2\pi - \Phi). \quad (8)$$

Then, using the known properties of the spherical harmonics,

$$Y_{LM}(\pi - \Theta, \Phi) = (-1)^{L+M}Y_{LM}(\Theta, \Phi), \quad (9)$$

$$Y_{LM}(\Theta, 2\pi - \Phi) = Y_{LM}^*(\Theta, \Phi), \quad (10)$$

one can see that the relations (8) lead to the following restrictions for the coefficients W_{LM}:

$$W_{LM} = 0, \quad \text{if} \quad L + M = \text{odd}, \quad (11)$$

and

$$\text{Im}(W_{LM}) = 0. \quad (12)$$

In particular, $W_{L0} = 0$ for $L = 2n + 1$. Furthermore, parity conservation requires that the amplitudes with the same parity interfere only in W_{LM} with even L, whereas the waves having the opposite parity interfere only in W_{LM} with odd L. This property was effectively used in partial-wave analyses of inelastic pion-nucleon scattering $\pi N \to \pi\pi N$ [24,25].

The rule (11) requires that, for example, the states with $J^P = \frac{1}{2}^+$ produced via $M1$ absorption (which in our case is saturated by the Roper resonance and by the major part of the Born terms) can contribute only to W_{00}. Therefore, in the region where states with $J \geqslant 3/2$ are not important, the angular distribution $W(\Theta, \Phi)$ should be isotropic in both Θ and Φ.

V. DISCUSSION OF THE RESULTS

The measured distributions of the angles Θ and Φ defined in Sec. IV are shown in Figs. 4 and 5 for 50-MeV-wide energy bins. The predictions that were made for these angular distributions by the model from Ref. [19] are shown in the same figures by dashed lines. This model describes roughly the experimental distributions in the energy region close to $D_{13}(1520)$. At the energies below $E_\gamma = 900$ MeV, the shape of the measured $\cos\Theta$ distributions shows good agreement with formula (6). However, at the energies below $D_{13}(1520)$, where the model of Ref. [19] involves the $P_{11}(1440)$ resonance and the nucleon Born terms come into play, the model predicts an angular dependence that is weaker compared to the experimental data. As follows from Eq. (6), the weakening of the moment W_{20} leads to the model failure at these energies. Within our approximation $J \leqslant 3/2$, this moment is saturated by the waves corresponding to the total angular momentum $J = 3/2$. Therefore, this observation indicates the persistence of such waves (and perhaps higher waves) at these energies. As already discussed in Sec. I, the Roper resonance cannot dominate at these energies. At the same time, the calculations from Refs. [12,17,19] predict a rapid fall of
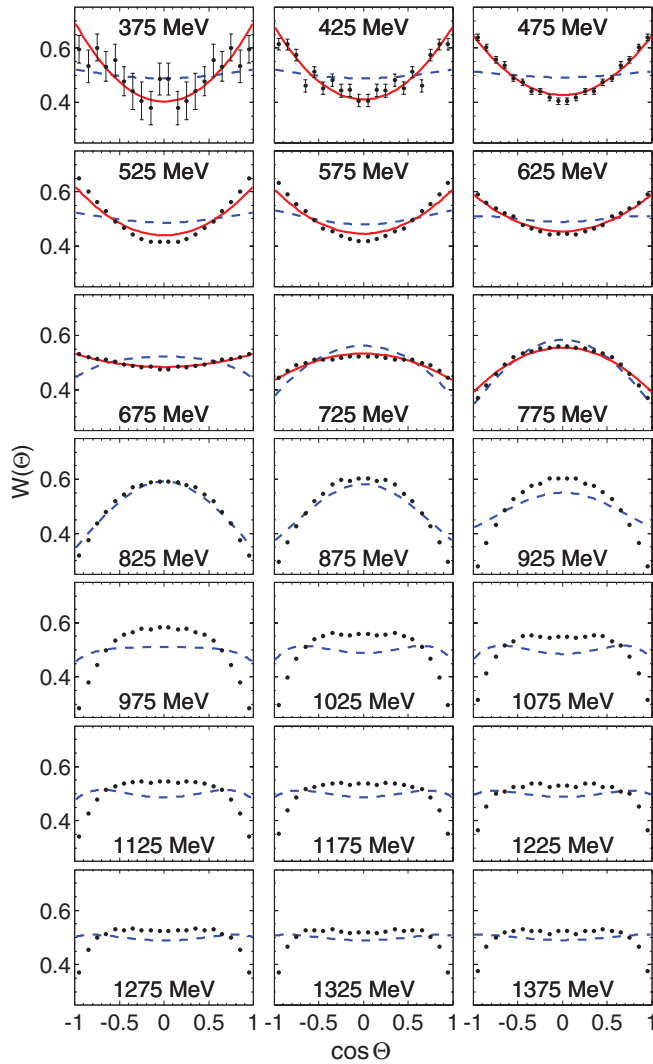
FIG. 4. (Color online) Distribution $W(\Theta) = \int W(\Theta, \Phi) d\Phi$ shown as a function of $\cos \Theta$, where Θ is the polar angle of the incident photon in the coordinate frame presented in Fig. 3. Our experimental results with statistical uncertainties are shown by filled circles. The predictions from the model of Ref. [19] are shown by dashed lines. The results of fitting our data below $E_\gamma = 0.8$ GeV are shown by solid lines. The energy label in each panel indicates the central photon energy for each bin.
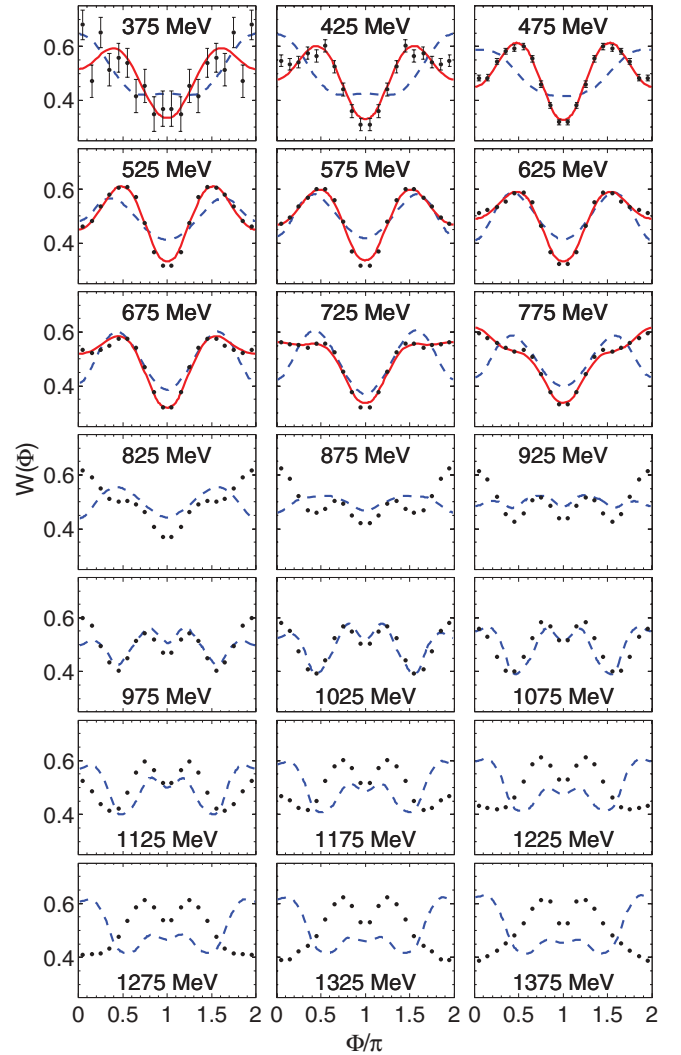
FIG. 5. (Color online) Distribution $W(\Phi) = \pi \int W(\Theta, \Phi) \sin \Theta \, d\Theta$, where Φ is the azimuthal angle of the incident photon in the coordinate frame presented in Fig. 3. Other notations are the same as in Fig. 4.

the $D_{13}(1520)$ contribution at lower energies. This results in the significant underestimation of the measured total cross section, which demonstrates almost linear energy dependence in this region. According to the fit of Ref. [12], such behavior of the experimental data was explained by a contribution from the Δ-like resonance $D_{33}(1700)$, which dominated the $\pi^0\pi^0$ channel in the full energy region considered.

Using Eq. (3), the expansion coefficients W_{LM} were obtained from the experimental two-dimensional plots of $\cos \Theta$ versus Φ. To illustrate the partial-wave content of the $\gamma p \to \pi^0 \pi^0 p$ amplitude in more detail, we show in Fig. 6 the variation of these coefficients in the energy range $E_\gamma = 400$– 1400 MeV for the waves with $J \leqslant 5/2$. As remarked above, the values of the coefficients with odd J are determined by

the interference of the states with different parities. If the insignificance of the waves with $J > 3/2$ is assumed, nonzero W_{3M} coefficients arise from the interference between $3/2^-$ and $3/2^+$. As one can see in Fig. 6, W_{31} and W_{33} are quite small. This observation, for example, may point to a predominantly background nature of the partial wave with $J^P = 3/2^+$, which thus has a small imaginary part, whereas $J^P = 3/2^-$ is mostly imaginary because of the closeness to the $D_{13}(1520)$ pole. Furthermore, as will be shown later, the weakness of the interference between $3/2^-$ and the positive-parity states $1/2^+$ and $3/2^+$ results in a small forward-backward asymmetry in the angular distributions for the final-state pions.

Already at low energies, the quantities W_{20} and W_{22}, which (within our restriction $J \leqslant 3/2$) are determined exclusively by the incoherent sum of the states $3/2^-$ and $3/2^+$, achieve relatively large values. This observation indicates an additional strong $3/2^-$ contribution, interfering with $D_{13}(1520)$, and/or a large fraction of $3/2^+$. The latter can come, for example,
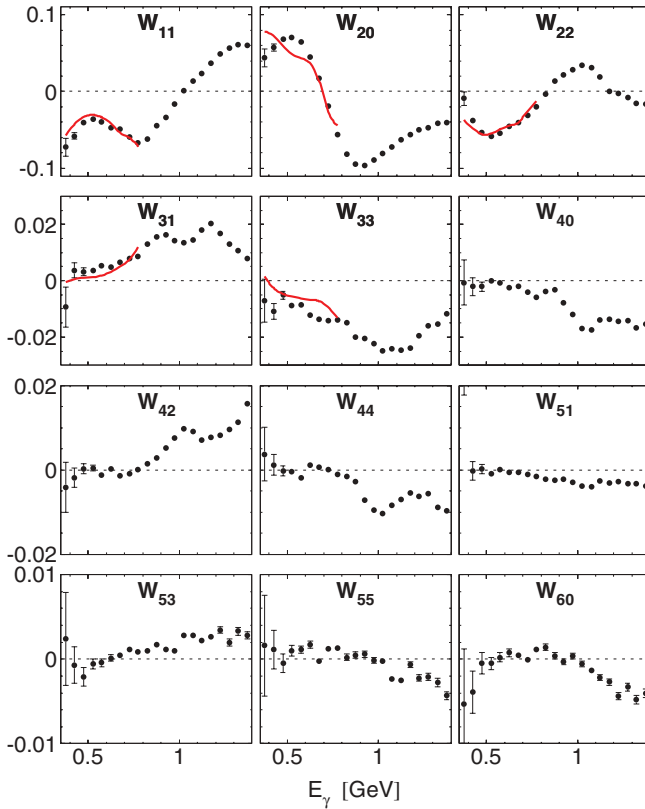
FIG. 6. (Color online) Moments W_{LM} (normalized such that $W_{00} = 1$) as a function of the incident-photon energy. Our experimental results for the real part of W_{LM} are shown by filled circles. The fit results are shown by solid lines.
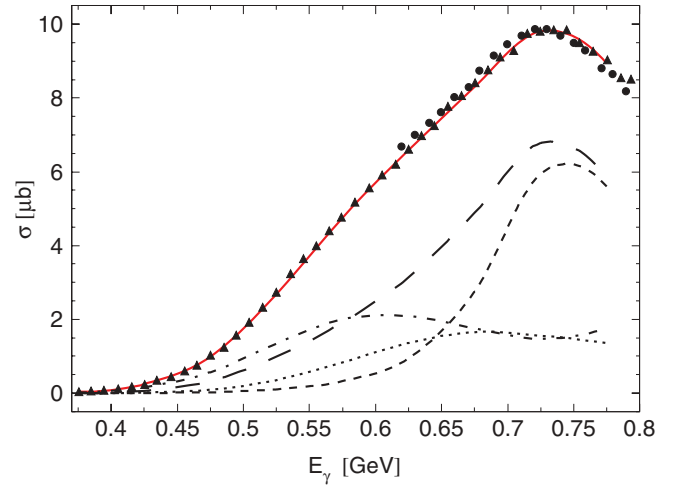

FIG. 7. (Color online) Total cross section for $\gamma p \rightarrow \pi^0 \pi^0 p$ as a function of the incident-photon energy. Our experimental results are shown by triangles and circles, respectively, for the data with the 855- and 1508-MeV electron beams. Only statistical uncertainties are shown. The fit results for the total cross section are shown by the solid line, and for the $3/2^-$, $3/2^+$, and $1/2^+$ waves by long-dashed, dash-dotted, and dotted lines, respectively. The $D_{13}(1520)$ contribution, calculated from the model of Ref. [19], is shown by the short-dashed line.

from Δ decaying to $\pi \Delta$, followed by $\Delta \rightarrow \pi N$. We cannot also exclude a strong $D_{33}(1700)$ amplitude, as was found in Ref. [12]. However, as discussed in Sec. I, the experimental data on $\pi^+\pi^-$ photoproduction seem to leave no room for strong coupling to this resonance.

The coefficient W_{11}, coming from the interference of the $3/2^-$ wave with the positive-parity waves $1/2^+$ and $3/2^+$, demonstrates quite sharp energy dependence in the region $E_\gamma = 500$–650 MeV. The moments with $L = 5$ are small.

To fit the measured values of the moments W_{LM}, we assumed the model in which the final $\pi \pi N$ state is produced exclusively via the intermediate $\pi \Delta$ state. First, the resonance $D_{13}(1520)$, whose role in this reaction is more or less firmly established, was put into the $3/2^-$ wave. The corresponding amplitude was parametrized in the Breit-Wigner form, with parameters taken from PDG [38]. The only other partial waves included were those that lead to s and p wave in the final $\pi \Delta$ state: $J^P = 1/2^+$, $3/2^-$, and $3/2^+$. From our fit, the wave $J^P = 5/2^+$, containing $\pi \Delta$ in a p state, is negligibly small and was excluded from further consideration. Each partial-wave amplitude was parametrized in the form

$$t_{J^P} = [t_B + t_R(W)]\, G_\Delta F_{\Delta \rightarrow \pi N}\,, \qquad (13)$$

where the two terms in the brackets stand for a smooth background and a rapidly-varying part $t_R(W)$, which can contain s-channel resonances. The factors G_Δ and $F_{\Delta \rightarrow \pi N}$ are

respectively the propagator and the πN-decay vertex of the Δ isobar. The energy-independent background in each partial wave was parametrized as

$$t_B = |t_B| e^{i\phi_B}\,, \qquad (14)$$

with adjustable constants $|t_B|$ and ϕ_B, whereas the rapidly varying part was taken as

$$t_R(W) = |t_R(W)| e^{i\phi_R(W)} \qquad (15)$$

with

$$|t_R(W)| = a_0 + a_1 q + a_2 q^2, \quad \phi_R(W) = \frac{q^3}{b_1 + b_2 q^2}, \quad (16)$$

where q is the maximum pion momentum in the final $\pi \pi N$ state, corresponding to the total energy W in the center-of-mass system:

$$q = \frac{\sqrt{\left(W^2 - (M_N + 2m_\pi)^2\right)\left(W^2 - M_N^2\right)}}{2W}\,. \qquad (17)$$

The coefficients a_i and b_i in Eq. (16) should be determined from the fit. Since our fit was restricted to a limited energy range, the parametrization of $|t_R(W)|$ by a simple polynomial formula (16) was expected to be satisfactory.

The results of the fit to the W_{LM} moments are shown by solid lines in Fig. 6. Instead of listing the results for the fit parameters, the integrated partial cross sections σ_{J^P} are shown in Fig. 7. As expected, the strongest $\pi^0 \pi^0$ production into the entire energy region comes from $J^P = 3/2^-$ and $3/2^+$ (shown by the long-dashed and dash-dotted lines in Fig. 7). At lower photon energy energies the partial cross section $\sigma_{3/2^-}$ falls off slower than predicted by the model [19]. In addition, the wave
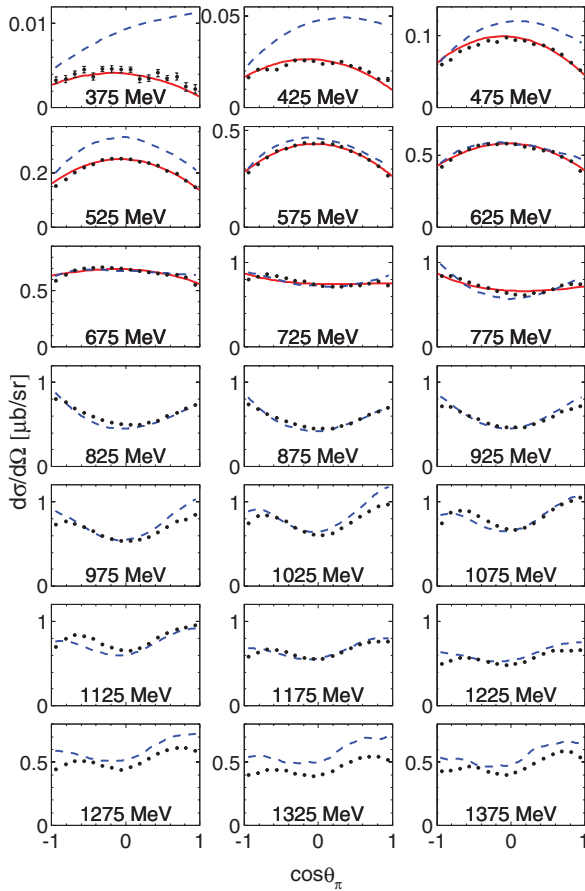
FIG. 8. (Color online) $\gamma p \rightarrow \pi^0 \pi^0 p$ differential cross sections as a function of the production angle of the outgoing π^0 in the center of mass frame. Since there are two identical pions, each cross section represents the average of two distributions. Our experimental results with statistical uncertainties are shown by filled circles. The predictions from our model are shown by solid lines. The dashed lines result from the Bonn-Gatchina model [11,12].

FIG. 9. (Color online) Same as Fig. 8 but for the outgoing proton.

$3/2^+$ turns out to be very important, especially at the energies below $E_\gamma = 650$ MeV.

After fitting the model parameters to the measured total cross sections and moments W_{LM}, the reliability of our parametrization [given by Eqs. (13)–(16)] was checked by comparing the model predictions with the $\gamma p \rightarrow \pi^0 \pi^0 p$ experimental results for other observables. These comparisons are shown in Figs. 8–13. Before discussing the agreement between the experimental data and the calculation, it is important to note that the values of W_{LM} do not determine final-state distributions of $\gamma p \rightarrow \pi^0 \pi^0 p$ [because of the integration over energies ω_1 and ω_2 in Eq. (3)]. Therefore, the theoretical results shown in Figs. 8–13 depend essentially on the model used for describing the production mechanism. As discussed above, we used the assumption that the $\gamma p \rightarrow \pi^0 \pi^0 p$ reaction proceeds exclusively through the transition $\Delta \pi \rightarrow \pi \pi N$. Agreement with the measurements would support this asumption.

In Figs. 8 and 9, we show our experimental results for the $\gamma p \rightarrow \pi^0 \pi^0 p$ differential cross sections as a function of the production angle of the outgoing π^0 and proton in the center-of-mass frame. Figures 10 and 11 show our differential cross
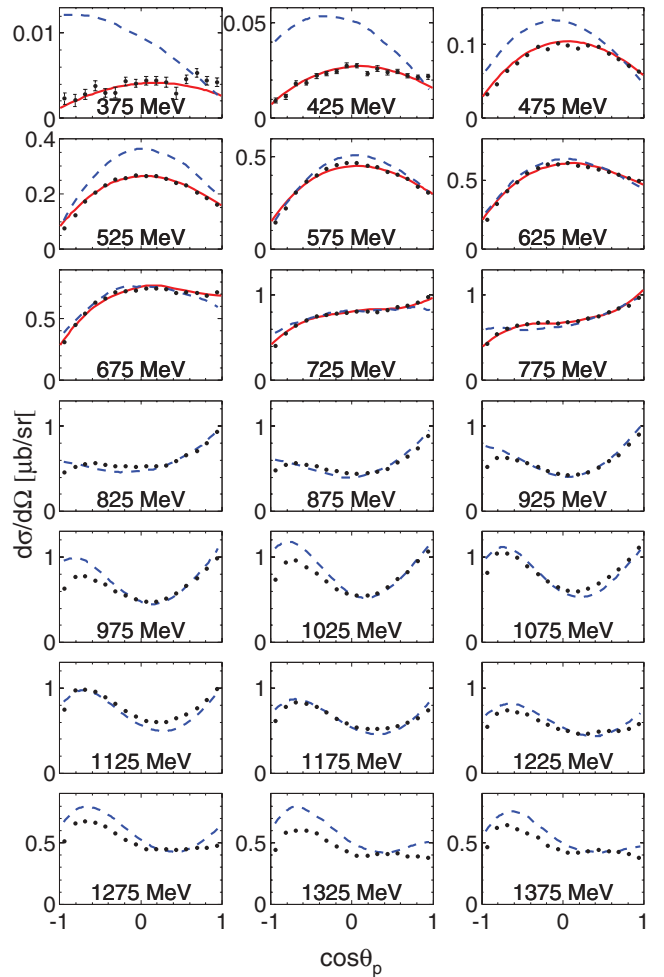
sections as a function of the invariant mass squared $m^2(\pi^0 \pi^0)$ and $m^2(\pi^0 p)$. These results are obtained for the same energies that were used for the angular distribution, shown in Figs. 4 and 5. The model predictions are shown in these figures up to $E_\gamma = 775$ MeV. They are in reasonable agreement with the experimental results, especially concerning the shape of the angular distributions. In particular, the calculations reproduce not only the convexity and its sign, which changes with energy, but also the forward-backward asymmetry. This asymmetry is mostly determined by the interference of the $3/2^-$ wave with positive-parity waves (in our case $1/2^+$ and $3/2^+$). As discussed above, the smallness of this forward-backward asymmetry indicates the weakness of this interference. This is also related to the small values of the moments W_{3M}, shown in Fig. 6.

The model predictions for the invariant-mass distributions, shown in Figs. 10 and 11, are not so impressive. The poorer level of agreement could be partially explained by pion rescattering in the final state, which was neglected in our model. According to Refs. [41,42], the pion loops in the $\pi^0 \pi^0$ channel can lead to a significant enhancement of the cross section at low energies. This is primarily because of a large yield of $\pi^+ \pi^-$ pairs, which in turn can rescatter into neutral pions. As known, the interaction between pions in the
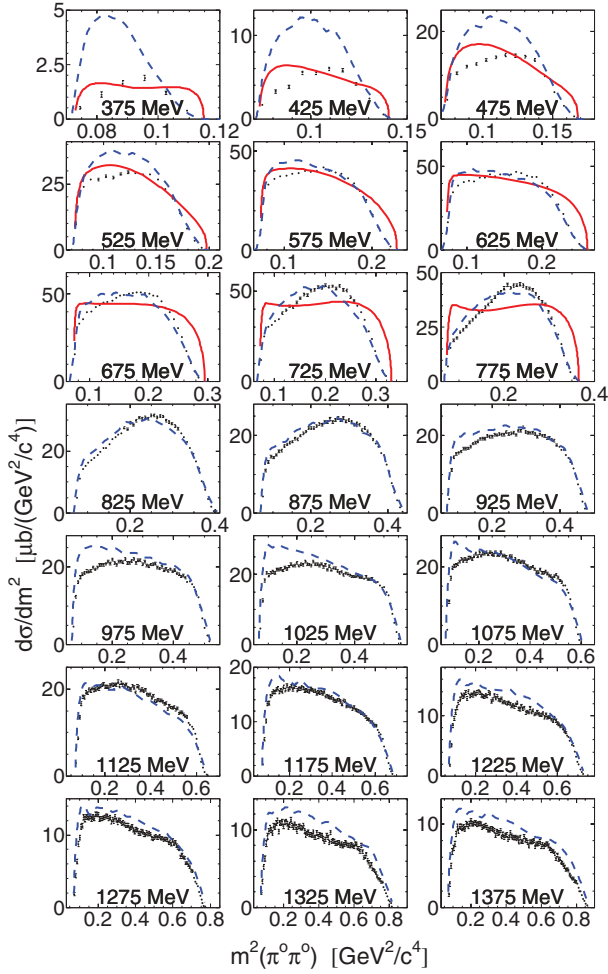
FIG. 10. (Color online) $\gamma p \rightarrow \pi^0 \pi^0 p$ differential cross sections as a function the invariant mass squared, $m^2(\pi^0\pi^0)$. Our experimental results with statistical uncertainties are shown by filled circles. The predictions from our model are shown by solid lines. The dashed lines result from the Bonn-Gatchina model [11,12].

state $J^P = 0^+$, $I = 0$ is attractive. The corresponding phase shift reaches $\pi/2$ close to $M_{\pi\pi} = 900$ MeV (see Ref. [43]). Therefore, it is reasonable to expect that the inclusion of this effect will shift the $m(\pi^0\pi^0)$ spectrum to higher masses. Another possible reason for the poor agreement is that the fraction of the wave $J^P = 1/2^+$ in our model is slightly overestimated. If the $\pi\pi$ system does not resonate [or the $\pi\pi$ resonance is wide, like $f_0(600)$], then the shape of the Dalitz plot $(M^2_{\pi\pi}, M^2_{\pi p})$ is totally determined by the spin parity J^P of a given partial wave (see the corresponding discussion for $\pi^0\eta$ photoproduction in Ref. [44]). To illustrate this statement, the contributions of the individual states to the $\pi\pi$ spectrum are shown in Fig. 12 for $E_\gamma = 425$ and 775 MeV. The predicted enhancement of the cross section at the boundaries of the kinematical region, which is typical for the contribution from the state $J^P = 1/2^+$, is not exhibited by the experimental data. In this respect, our experimental results prefer a $1/2^+$ fraction that is even smaller than predicted by the fit of the moments W_{LM}.
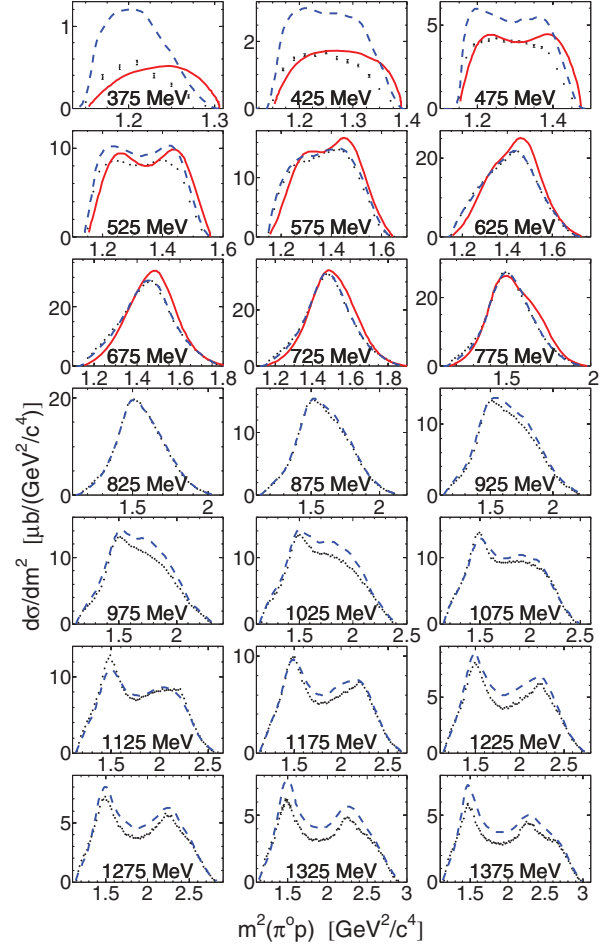

FIG. 11. (Color online) Same as Fig. 10, but for $m^2(\pi^0 p)$. Since there are two identical pions, each cross section represents the average of two distributions.

In Figs. 8 to 11, our experimental results are also compared to the predictions of the Bonn-Gatchina model [11,12]. The approach of Refs. [11,12] is based on the event-by-event likelihood fit that allows one to take accurately into account the correlations between the different reaction channels, for
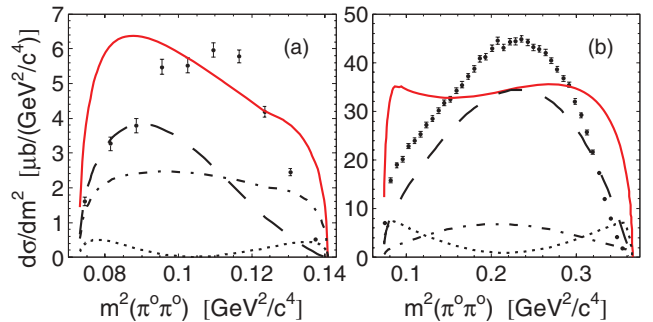

FIG. 12. (Color online) The partial-wave contributions to the $\pi\pi$ spectrum for $E_\gamma = 425$ (a) and 775 MeV (b) (enlarged from Fig. 10). Long-dashed, dash-dotted, and dotted lines correspond to the $3/2^-$, $3/2^+$, and $1/2^+$ waves, respectively. The sum of all waves is shown by solid lines.
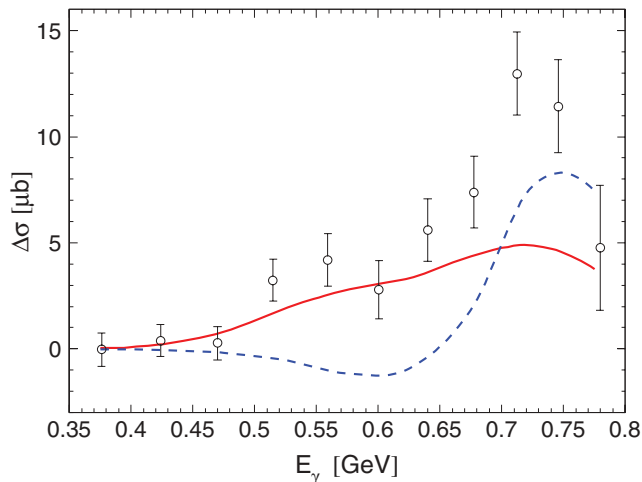
FIG. 13. (Color online) Helicity asymmetry $\Delta\sigma = \sigma_{3/2} - \sigma_{1/2}$ for $\gamma p \to \pi^0\pi^0 p$. The experimental data from Ref. [8] are shown by open circles. The prediction is shown by the solid line for our model, and by the dashed line for the isobar model of Ref. [19].

example, $\pi\Delta$ and σN. As one can see, the model from Refs. [11,12] describes our experimental results quite well above 550 MeV. Only at low E_γ does it overestimate the measured cross sections.

In Fig. 13, the prediction of our model for the $\Delta\sigma = \sigma_{3/2} - \sigma_{1/2}$ helicity asymmetry is compared to the $\gamma p \to \pi^0\pi^0 p$ experimental data from Ref. [8]. The experimental data, measured as the difference between the total cross sections with the initial γp-system helicity 3/2 and 1/2, indicate the dominance of the $\lambda = 3/2$ component over $\lambda = 1/2$ in the energy region $W = 1400$–1500 MeV, excluding any large contribution from the $J = 1/2$ waves. Our model reproduces the general trend of the data, which shows $\sigma_{3/2}$ dominance. The isobar model of Ref. [19], in which the Roper resonance was rather important in the region $E_\gamma = 500$–600 MeV, predicts negative values for $\Delta\sigma$ (shown by the dashed line in the same figure). In this energy region, this is in contradiction with the experimental data.

VI. SUMMARY AND CONCLUSIONS

The $\gamma p \to \pi^0\pi^0 p$ reaction has been measured at the tagged-photon facility of the Mainz Microtron MAMI-C

using the Crystal Ball and TAPS spectrometers. The experimental results, obtained from the production threshold up to a photon energy of 1.4 GeV, include the total cross sections, various differential cross sections, and specific angular distributions. The moments W_{LM} obtained from these angular distributions were used to study the importance of different partial waves in double-π^0 photoproduction at energies below $D_{13}(1520)$ (a region that has not been so far fully understood theoretically). The reliability of our model was checked by the comparison of its predictions with the $\gamma p \to \pi^0\pi^0 p$ experimental results for other observables.

Our analysis of the energy dependence of W_{LM} showed that a large contribution from the $J = 3/2$ waves is necessary, not only in the region of $D_{13}(1520)$ but also at energies below. According to our results, these waves seem to be responsible for an almost linear rise of the $\gamma p \to \pi^0\pi^0 p$ total cross section in the region $E_\gamma = 450$–725 MeV. Isobar models with the dominant contribution from $D_{13}(1520)$ and a moderate role for the Roper resonance cannot explain such features in double-π^0 photoproduction. Whether these features are the reflection of a large $J^\pi = 3/2^+$ fraction of $\pi^+\pi^- \to \pi^0\pi^0$ rescattering, or are a consequence of the strong $D_{33}(1700)$ excitation, found in Ref. [12], requires further experimental and theoretical studies.

[1] A. Braghieri *et al.*, Phys. Lett. B **363**, 46 (1995).

[2] F. Härter *et al.*, Phys. Lett. B **401**, 229 (1997).

[3] M. Wolf *et al.*, Eur. Phys. J. A **9**, 5 (2000).

[4] W. Langgärtner *et al.*, Phys. Rev. Lett. **87**, 052001 (2001).

[5] J. Ahrens *et al.*, Phys. Lett. B **551**, 49 (2003).

[6] Y. Assafiri *et al.*, Phys. Rev. Lett. **90**, 222001 (2003).

[7] M. Kotulla *et al.*, Phys. Lett. B **578**, 63 (2004).

[8] J. Ahrens *et al.*, Phys. Lett. B **624**, 173 (2005).

[9] S. Strauch *et al.*, Phys. Rev. Lett. **95**, 162003 (2005).

[10] J. Ahrens *et al.*, Eur. Phys. J. A **34**, 11 (2007).

[11] U. Thoma *et al.*, Phys. Lett. B **659**, 87 (2008).

[12] A. V. Sarantsev *et al.*, Phys. Lett. B **659**, 94 (2008).

[13] D. Krambrich *et al.*, Phys. Rev. Lett. **103**, 052002 (2009).

[14] J. G. Messchendorp *et al.*, Phys. Rev. Lett. **89**, 222302 (2002).

[15] J. A. Gomez Tejedor and E. Oset, Nucl. Phys. A **600**, 413 (1996).

[16] L. Y. Murphy and J. M. Laget, DAPHNIA/SPhN Report No. 96-10, 1996 (unpublished).

[17] K. Ochi, M. Hirata, and T. Takaki, Phys. Rev. C **56**, 1472 (1997).

[18] M. Ripani *et al.*, Nucl. Phys. A **672**, 220 (2000).

[19] A. Fix and H. Arenhövel, Eur. Phys. J. A **25**, 115 (2005).

[20] H. Kamano, B. Julia-Diaz, T. S. H. Lee, A. Matsuyama, and T. Sato, Phys. Rev. C **80**, 065203 (2009).

[21] D. M. Manley and E. M. Saleski, Phys. Rev. D **45**, 4002 (1992).

[22] T. P. Vrana, S. A. Dytman, and T. S. H. Lee, Phys. Rep. **328**, 181 (2000).

[23] L. Roca, Nucl. Phys. A **748**, 192 (2005).

[24] R. C. Arnold and J. L. Uretsky, Phys. Rev. **1443**, 153 (1967).

[25] D. Morgan, Phys. Rev. **166**, 1731 (1968).

[26] A. Fix and H. Arenhövel, arXiv:1201.5739 [nucl-th].

[27] A. Starostin *et al.*, Phys. Rev. C **64**, 055205 (2001).

[28] R. Novotny, IEEE Trans. Nucl. Sci. **38**, 379 (1991).

[29] A. R. Gabler *et al.*, Nucl. Instrum. Methods A **346**, 168 (1994).

[30] H. Herminghaus *et al.*, IEEE Trans. Nucl. Sci. **30**, 3274 (1983).

[31] K.-H. Kaiser *et al.*, Nucl. Instrum. Methods A **593**, 159 (2008).

[32] J. C. McGeorge *et al.*, Eur. Phys. J. A **37**, 129 (2008).

[33] I. Anthony *et al.*, Nucl. Instrum. Methods A **310**, 230 (1991).

[34] S. J. Hall *et al.*, Nucl. Instrum. Methods A **368**, 698 (1996).

[35] S. Prakhov *et al.*, Phys. Rev. C **79**, 035204 (2009).

[36] E. F. McNicoll *et al.*, Phys. Rev. C **82**, 035208 (2010).

[37] V. L. Kashevarov *et al.*, Eur. Phys. J. A **42**, 141 (2009).

[38] K. Nakamura *et al.* (Particle Data Group), J. Phys. G **37**, 075021 (2010).

[39] S. Prakhov *et al.*, Phys. Rev. C **69**, 045202 (2004).

[40] S. Schuman *et al.*, Eur. Phys. J. A **43**, 269 (2010).

[41] V. Bernard, N. Kaiser, and U.-G. Meissner, Phys. Lett. B **382**, 19 (1996).

[42] L. Roca, E. Oset, and M. J. Vicente Vacas, Phys. Lett. B **541**, 77 (2002).

[43] S. D. Protopopescu *et al.*, Phys. Rev. D **7**, 1279 (1973).

[44] A. Fix, M. Ostrick, and L. Tiator, Eur. Phys. J. A **36**, 61 (2008).